Experimental Neurology 313 (2019) 124–134

Contents lists available at ScienceDirect

Experimental Neurology

journal homepage: www.elsevier.com/locate/yexnr

Research paper

Daily acute intermittent hypoxia induced dynamic changes in dendritic mitochondrial ultrastructure and cytochrome oxidase activity in the pre-Bötzinger complex of rats

Jun-Jun Kang[a,1], Baolin Guo[a,1], Wei-Hua Liang[b], Chun-Sing Lam[c], Sheng-Xi Wu[a], Xiao-Feng Huang[b], Margaret T.T. Wong-Riley[d], Man-Lung Fung[c,**], Ying-Ying Liu[a,*]

[a] Department of Neurobiology, The Fourth Military Medical University, Xi'an 710032, PR China
[b] Department of Pathology and Pathophysiology, The Fourth Military Medical University, Xi'an 710032, PR China
[c] School of Biomedical Sciences, The University of Hong Kong, PR China
[d] Department of Cell Biology, Neurobiology and Anatomy, Medical College of Wisconsin, Milwaukee, WI 53226, USA

ARTICLE INFO

Keyworks:
Neuroplasticity
Mitochondria
Cytochrome oxidase
Pre-Bötzinger complex
Dendrite
Intermittent hypoxia
Immuno-electron microscope

ABSTRACT

Mitochondria, as primary energy generators and Ca^{2+} biosensor, are dynamically coupled to neuronal activities, and thus play a role in neuroplasticity. Here we report that respiratory neuroplasticity induced by daily acute intermittent hypoxia (dAIH) evoked adaptive changes in the ultrastructure and postsynaptic distribution of mitochondria in the pre-Bötzinger complex (pre-BötC). The metabolic marker of neuronal activity, cytochrome *c* oxidase (CO), and dendritic mitochondria were examined in pre-BötC neurons of adult Sprague-Dawley rats preconditioned with dAIH, which is known to induce long-term facilitation (LTF) in respiratory neural activities. We performed neurokinin 1 receptor (NK1R) pre-embedding immunocytochemistry to define pre-BötC neurons, in combination with CO histochemistry, to depict ultrastructural alterations and CO activity in dendritic mitochondria. We found that the dAIH challenge significantly increased CO activity in pre-BötC neurons. Darkly CO-reactive mitochondria at postsynaptic sites in the dAIH group were much more prevalent than those in the normoxic control. In addition, the length and area of mitochondria were significantly increased in the dAIH group, implying a larger surface area of cristae for ATP generation. There was a fine, structural remodeling, notably enlarged and branching mitochondria or tapered mitochondria extending into dendritic spines. Mitochondrial cristae were mainly in parallel-lamellar arrangement, indicating a high efficiency of energy generation. Moreover, flocculent or filament-like elements were noted between the mitochondria and the postsynaptic membrane. These morphological evidences, together with increased CO activity, demonstrate that dendritic mitochondria in the pre-BötC responded dynamically to respiratory plasticity. Hence, plastic neuronal changes are closely coupled to active mitochondrial bioenergetics, leading to enhanced energy production and Ca^{2+} buffering that may drive the LTF expression.

1. Introduction

Mitochondria, as primary energy generators, are dynamic in structure and function and are abundantly found in neurons for supporting high ATP consumption (Barnhart, 2016). About one-tenth of the gray matter volume is occupied by mitochondria, which are responsible for > 90% of ATP production in neurons. Mitochondria are located mainly in subcellular regions, especially at synapses where energy demands are the highest (Harris et al., 2012). Additionally, mitochondria efficiently buffer intracellular calcium to enable intrinsic activities and signaling processes (Gunter et al., 2000; Billups and Forsythe, 2002). Since synaptic processes are highly energy-consuming, mitochondria, as neuronal power plants and calcium regulators, are pivotal in synaptic function and neuroplasticity (Cheng et al., 2010). Previous studies

Abbreviations: BSA, bovine serum albumin; CO, cytochrome *c* oxidase; dAIH, daily acute intermittent hypoxia; ir, immunoreactive; LTF, long-term facilitation; NK1R, neurokinin 1 receptor; NGS, normal goat serum; PB, phosphate buffer; PBS, phosphate buffered saline; pre-BötC, pre-Bötzinger complex

* Correspondence to: Y. Liu, Department of Neurobiology, The Fourth Military Medical University, 169 Chang Le Xi Road, Xi'an 710032, PR China.
** Correspondence to: M. Fung, School of Biomedical Sciences, 21 Sassoon Road, Pokfulam, The University of Hong Kong, Hong Kong, PR China.
E-mail addresses: fungml@hku.hk (M.-L. Fung), yingyliu@fmmu.edu.cn (Y.-Y. Liu).

[1] These authors contribute equally to this work

https://doi.org/10.1016/j.expneurol.2018.12.008
Received 8 November 2018; Accepted 18 December 2018
Available online 23 December 2018
0014-4886/ © 2018 Elsevier Inc. All rights reserved.

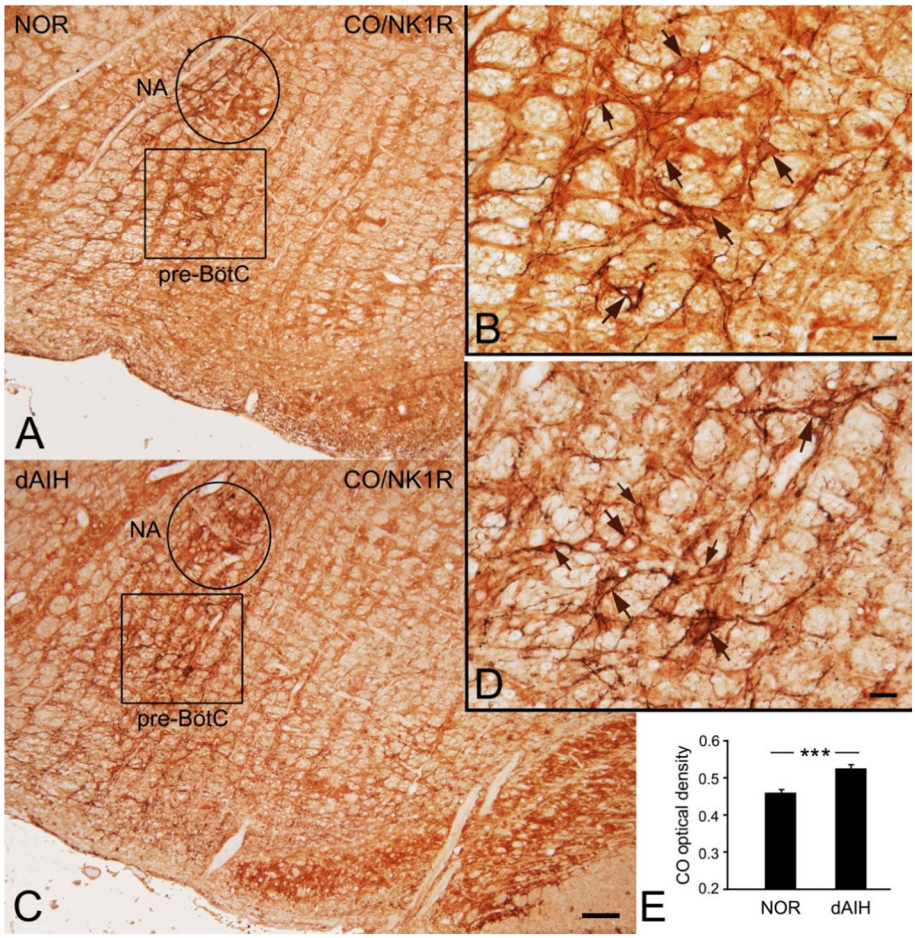

Fig. 1. Low magnification photomicrographs of the pre-Bötzinger complex (pre-BötC, boxes) and the nucleus ambiguus (NA, circles) in coronal sections of brainstems in normoxic (NOR, A) and daily acute intermittent hypoxic (dAIH, C) groups. B and D represent higher magnifications of neurons in boxes in A and C, respectively. Sections were double-labeled with neurokinin-1 receptor (NK1R) immunoreactivity and cytochrome *c* oxidase (CO) histochemistry. Double labeled neurons were small (thin arrows) and medium (thick arrows) in size with long processes. NK1R immunoreactivity was present mainly on the membranes of the somata and processes, and CO reactivity appeared in the cytoplasm and processes (B, D). Optical densitometric measurements of CO reaction product showed a significant increase in CO activity in the pre-BötC in the dAIH group (E, Mann-Whitney *U* test, U = 761, $p < 0.001$). Scale bars for A and C: 250 μm, for B and D: 25 μm, ***: $p < 0.001$.

showed that changes in mitochondria are associated with long-term potentiation of synaptic transmission, a key process in learning and memory (Li and Sheng, 2012; Smith et al., 2016). Loss of mitochondria in axonal terminals in *Drosophila* leads to defective synaptic transmission (Stowers et al., 2002). Mitochondrial calcium buffering is also closely coupled to presynaptic transmission and plasticity (Cai et al., 2011). Decreased capability of mitochondrial calcium buffering in dendrites in the hippocampus caused by impaired mitochondrial motility diminished synaptic plasticity and spontaneous synaptic activity (Ruggiero et al., 2017). A recent electron tomographic study revealed activity-dependent ultrastructural plasticity in axonal mitochondria, speculating that “stronger synapses use stronger mitochondria” (Cserep et al., 2018). While previous studies were largely focused on presynaptically-targeted mitochondria, less was explored on the postsynaptic counterparts, the dendritic mitochondria, especially at the ultrastructural level.

Respiration is an autonomous rhythmic process to regulate levels of oxygen and carbon dioxide in the blood and tissues, which sustains life (Xing et al., 2013). The respiratory system expresses diverse forms of plasticity (Mitchell and Johnson, 2003; Xing et al., 2013). The most frequently studied model is long-term facilitation (LTF), characterized as a progressive and sustained increase in respiratory motor output lasting for hours, which can be induced by repetitive hypoxia (Mitchell et al., 2001; Mitchell and Johnson, 2003). Daily acute intermittent hypoxic (dAIH) challenge, a well-established mild hypoxic paradigm, enables phrenic and hypoglossal nerves to express respiratory metaplasticity, which can promote respiratory and motor functional recovery after spinal cord injuries (Dale et al., 2014; Dougherty et al., 2017). Failure in LTF could lead to respiratory dysfunction, sudden infant death syndrome and obstructive sleep apnea syndrome.

The pre-Bötzinger complex (pre-BötC) located in the ventrolateral medulla is assumed to be essential for respiratory rhythmogenesis (Smith et al., 1991; Feldman et al., 2013). Neurons in the pre-BötC are heterogeneous and express high levels of neurokinin 1 receptors (NK1R). NK1R immunoreactivity has been used as a marker of the pre-BötC (Gray et al., 1999, 2001). The pre-BötC reconfigures to generate fictive eupnea under baseline condition and fictive gasping in hypoxia in isolated brainstem slices (Lieske et al., 2000), and it contributes to respiratory neuroplasticity (Barnett et al., 2017). A severe chronic intermittent hypoxic (CIH) challenge, mimicking a model of sleep apnea, increases baseline burst-to burst fluctuations or irregularity, and differentially imparts fictive states of inspiratory activity in the isolated pre-BötC (Garcia 3rd et al., 2016, 2017). We have shown structural and neurochemical evidence for altered neurotransmitters, receptors, and signaling in association with respiratory neuroplasticity in the pre-BötC induced by repetitive hypoxic challenge in rats (Wei et al., 2010; Kang et al., 2017). A question arises as to whether mitochondrial structure in the pre-BötC responds to respiratory neuroplasticity as a dynamic adaptation to the altered activity and energy demand. We are particularly interested in dendritic mitochondria at synapses, because energy consumption is mostly postsynaptically driven in dendrites (Wong-Riley, 1989), and there is a lack of ultrastructural evidence for dendritic mitochondrial plasticity. We hypothesized that dendritic mitochondrial dynamics with adaptive changes in ultrastructure in the pre-BötC are involved in respiratory neuroplasticity induced by dAIH challenge. We performed NK1R pre-embedding immunocytochemistry to define pre-BötC neurons, in combination with cytochrome *c* oxidase (CO) histochemistry, to depict ultrastructural alterations in dendritic mitochondria and CO activity in the pre-BötC in rats with dAIH preconditioning.

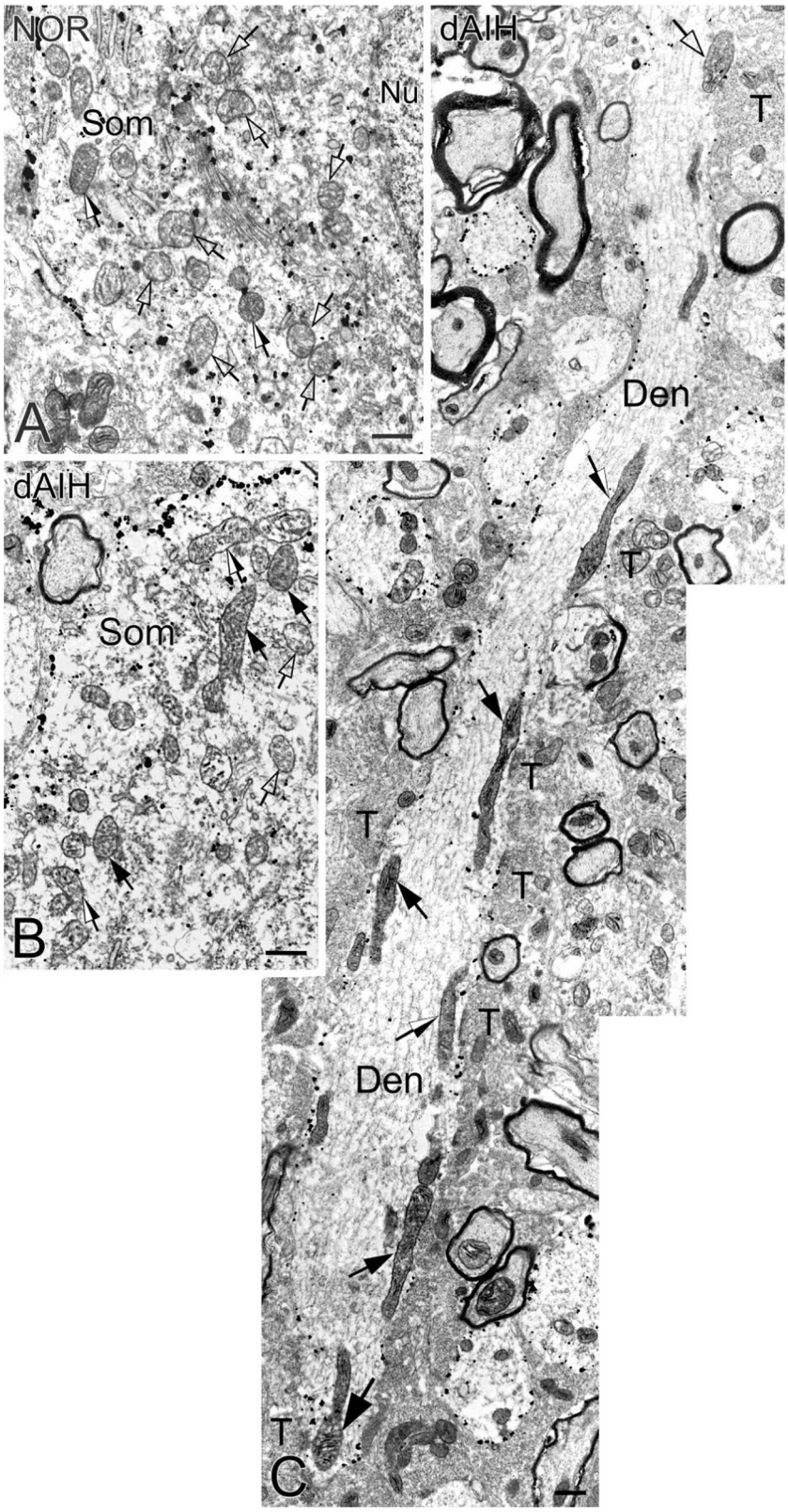

Fig. 2. Electron micrographs of CO– reactive mitochondria in the pre-BötC. Immunogold particles indicating NK1R immunoreactivity were localized mainly along the inner surface of membrane in the somata (A, B) and dendrites (C). The cytoplasm was also with NK1R immunoreactivity (A, B). Mitochondria with dark (solid arrows), moderate (half solid arrows), and light (open arrows) CO reactivity were shown in the somata (A, B) and dendrites (C). Dendritic mitochondria were longitudinally distributed in dendritic shafts and in close proximity to synapses (arrows in C). Note the enlarged portion of a mitochondrion (thick arrow in C). Som: soma, Den: dendrite, T: terminal. Nu: nucleus. Scale bars: 0.5 μm.

2. Materials and methods

Adult Sprague-Dawley rats (230–250 g) were housed in a room with a constant temperature and a 12 h light/dark cycle. Water and food were available ad libitum. All experimental procedures were approved by the Northwest China Committee of Experimental Animal Care; the Committee on the Use of Live Animals in Teaching and Research of the University of Hong Kong, and conformed to the Guide for the Care and Use of Laboratory Animals published by the National Institutes of Health (NIH). All efforts were made to minimize animal suffering and to reduce the number of animals used.

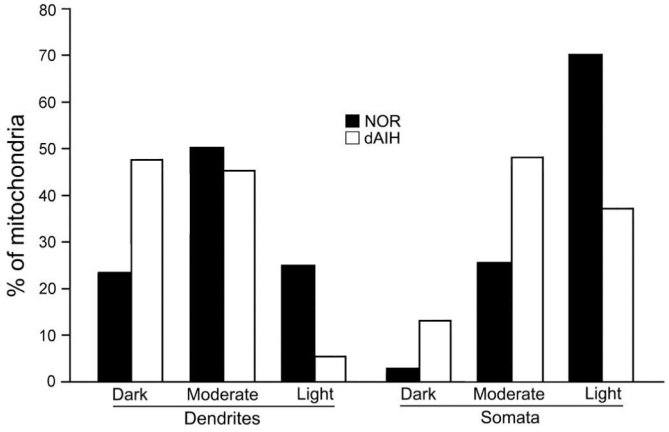

Fig. 3. Percent of darkly, moderately, and lightly reactive mitochondria in the pre-BötC in normoxic and dAIH groups. dAIH challenge increased darkly reactive mitochondria and reduced lightly reactive ones in dendrites and somata. An increase was also found in moderately reactive mitochondria in the somata of the dAIH group (open bars).

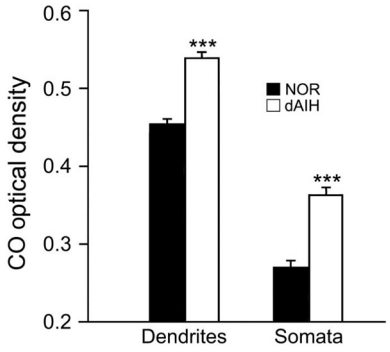

Fig. 4. Optical densitometric measurements of CO reaction product in dendrites and the somata of pre-BötC neurons in normoxic and dAIH groups. CO reactivity was significantly increased in dendrites and the somata of neurons in the dAIH (open bars) as compared to the normoxic group (solid bars). Mann-Whitney U test, Dendrites: U = 31, $p < 0.001$; Somata: U = 50, $p < 0.001$, ***: $p < 0.001$.

2.1. dAIH animal preparation

Animals were divided into normoxic and dAIH groups (twelve rats for each group). Normoxic rats were kept in room air, and dAIH rats were kept in an acrylic chamber for normobaric hypoxia. Hypoxic condition (10% O_2) was established with a mixture of room air and pure N_2, and monitored by an oxygen analyzer (Vacumetrics Inc., St. Ventura, CA, USA). The dAIH protocol consisted of ten 5-min episodes of hypoxia interspersed with 5-min room air intervals. Changes in O_2 levels in the chamber were reached within 20s during hypoxic episodes. Animals experienced dAIH protocol at 11:00 am each day for 7 days consecutively. The chamber was kept at a constant temperature (22 ± 1 °C) during the whole process. Animals were sacrificed 1 h after the last episode of intermittent hypoxia.

2.2. Histochemistry and immunogold-silver histochemstry

Eight rats from each group were perfused transcardially with 150 ml 0.9% saline followed by 500 ml ice cold 4% paraformaldehyde in 0.1 M phosphate buffer (PB, pH 7.4) for 30 min. Brainstems were removed and post-fixed in the same fixative for 1 h at 4 °C. They were then cryoprotected in 30% sucrose in 0.1 M PB overnight at 4 °C. Alternate sets of serial coronal sections of brainstems were cut at 12 μm thickness on a cryostat (CM1900, Leica, Heidelberger, Germany), and mounted on gelatin-coated slides for CO histochemistry and NK1R immunohistochemistry double staining. The basic protocol for CO histochemistry was as described previously (Liu and Wong-Riley, 2001; Liu et al., 2001). Briefly, slides were incubated in 0.1 M sodium phosphate buffer containing 25 mg 3, 3′-diaminobenzidine (Sigma, St. Louis, MO), 15 mg cytochrome *c*, type III (Sigma), and 2 g sucrose per 50 ml solution. They were incubated at 37 °C for 3 h in the dark. All slides from the two groups were reacted together to avoid differences due to slight variations, such as temperature, medium composition, or incubation time. After incubation, they were washed three times, 5 min each, in cold 0.1 M sodium phosphate buffer. CO-reacted slides were then conducted for NK1R immunohistochemistry staining. Slides were blocked for 2 h in phosphate buffered saline (PBS, pH 7.4), containing 5% bovine serum albumin (BSA), 5% normal goat serum (NGS), and 0.5% Triton X-100, and were then incubated overnight in the primary antibody of rabbit anti-NK1R (1:5000, S8305, Sigma), diluted in PBS containing 1% BSA, 1% NGS, and 0.5% Triton X-100. After rinsing in PBS, they were then incubated in anti-rabbit IgG conjugated to 1.4 nm gold particles (1:100, Nanoprobes, Stony Brook, NY) for 4 h. Silver enhancement was carried out in the dark with LI Silver Kit (Nanoprobes). Before and after the silver enhancement, slides were rinsed several times with deionized water. The sections were then dehydrated and cover-slipped for light microscopic observation. Image capturing was under a microscope (BX-51, Olympus, Tokyo, Japan).

Using NK1R immunoreactivity as a marker of the pre-BötC, CO activity was examined with identical conditions for quantitative densitometric measurements under a microscope (BX-51, Olympus), equipped with a 40× objective. They were imaged with a 12-bit color CCD camera (DP-70, Olympus), acquired at a resolution of 1360 × 1024 pixels, and stored in JEPG format. Twenty sections from each brainstem, a total of 160 sections from 8 normoxic or 8 dAIH animals, were collected and analyzed with Image-Pro Plus software (Media Cybernetics, Inc.). CO density was presented as mean ± SEM. Statistical significance was determined by Mann-Whitney *U* test. A *P* value of 0.05 or less was considered significant.

2.3. Pre-embedding immunogold-silver cytochemistry

Four rats from each group were deeply anesthetized with 1% sodium pentobarbital intraperitoneally (50 mg/kg body weight) and perfused transcardially with 150 ml saline, followed by 50 ml ice-cold mixture of 4% paraformaldehyde and 0.05% glutaraldehyde in 0.1 M PB for 1 h. Brainstems were removed and postfixed by immersion in the same fixative for 4 h at 4 °C. Serial coronal sections at 50 μm thicknesses were prepared with a vibratome (VS1000s, Leica, Heidelberger, Germany). Sections (n = 18–20) including the pre-BötC region were collected from each brainstem. CO histochemistry and NK1R immunocytochemistry double labeling was performed as described above with minimal modification that 0.05% Triton X-100 was used for NK1R immunogold-silver cytochemistry. After the second antibody incubation, sections were rinsed and postfixed in 2% glutaraldehyde in PBS for 45 min. Signals of NK1R immunoreactivity were detected by silver enhancement kit in the dark (HQ Silver Kit, Nanoprobes). Prior to, and after silver enhancing, sections were rinsed several times with deionized water. Sections were postfixed in 0.5% osmium tetroxide in 0.1 M PB for 2 h. They were then dehydrated with graded ethanol, replaced with propylene oxide, and finally embedded in Epon 812 between plastic sheets. After polymerization, flat-embedded sections were examined under the light microscope. Three to four sections containing NK1R immunoreactivity and CO activity in the pre-BötC were selected from each brainstem, trimmed under a stereomicroscope, and then glued onto blank resin stubs. Serial ultrathin sections were cut with a diamond knife (Diatome, Hatfield, PA) and mounted on formvar-coated mesh grids (6–8 sections/grid). They were then counterstained with uranyl acetate and lead citrate for the electron microscopic examination.

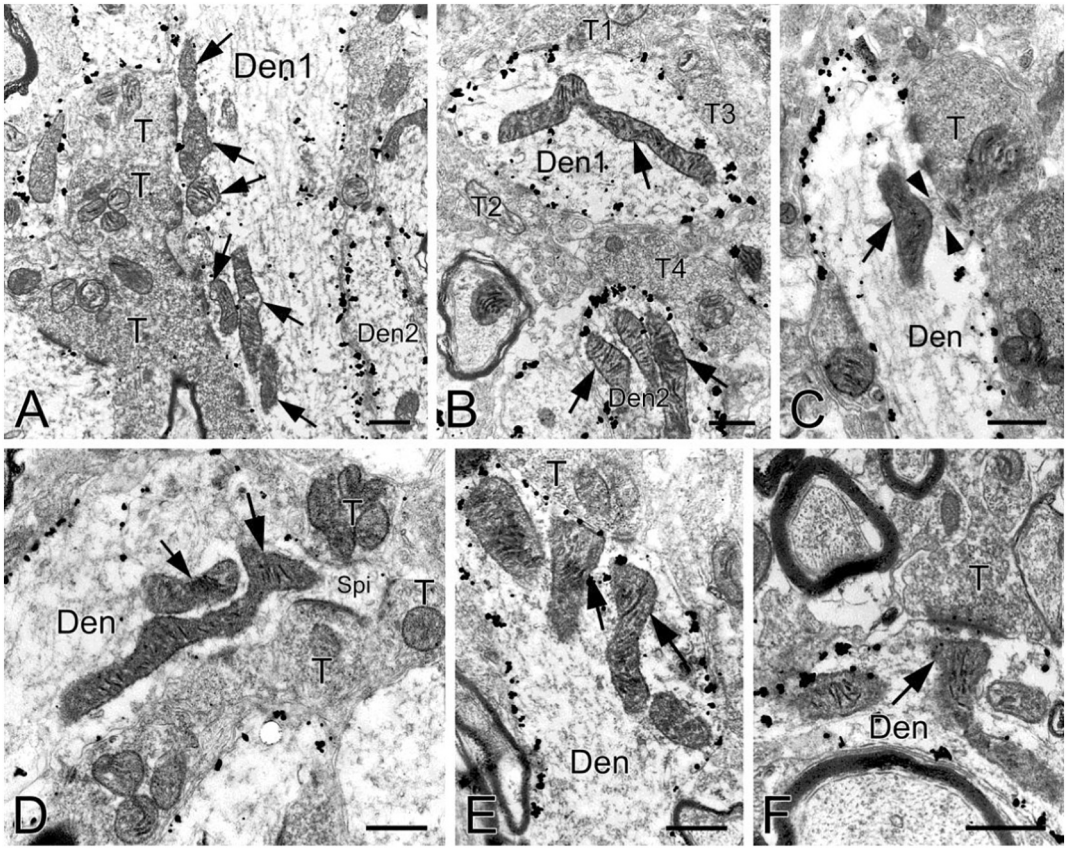

Fig. 5. Electron micrographs of CO-reactive mitochondria in dendrites of the pre-BötC in the normoxic group. Mitochondria were in close proximity to synapses (arrows). Relatively large mitochondria were observed at postsynaptic sites (arrows in C, E, F). An altered shape mitochondrion is extending toward a dendritic spine (thick arrow in D). Flocculent or filament-like elements were observed between the postsynaptic membrane and mitochondria (arrowheads in C). A mitochondrion was found in close proximity to an adjacent one (thin arrow in D). Den: dendrite, T: terminal, Spi: spine. Scale bars: 0.5 μm.

Ultrathin sections were examined under the JEM-1230 electron microscope (JEOL LTD, Tokyo, Japan) equipped with CCD camera and its application software (832 SC1000, Gatan, Warrendale, PA). 30 electron micrographs of postsynaptic dendrites and 8 of somata in the pre-BötC from one brainstem, a total of 120 of dendrites and 32 of somata from 4 normoxic or 4 dAIH animals were collected for quantitative analysis, respectively. In total, 2770 mitochondria, including 681 in dendrites and 692 in the somata in normoxic, and 688 dendritic and 709 somatic ones in dAIH groups were counted in the pre-BötC. Mitochondria in each electron micrograph were outlined along the membrane. The number, length, area, and density of CO reaction product, indicative of CO activity were obtained and analyzed with an Image-Pro Plus software (Media Cybernetics, Inc.), and presented as mean ± SEM. Statistical significance was determined by unpaired *t*-test and Mann-Whitney *U* test to identify individual comparisons. $P < 0.05$ or less was considered significant.

3. Results

3.1. Light microscopic examination of CO activity in the pre-BötC in normoxic and dAIH groups

The anatomical boundary of the pre-BötC, delineated by NK1R immunoreactivity, is located ventral to the nucleus ambiguus, caudal to the retrofacial nucleus, and rostral to the anterior tip of the lateral reticular nucleus, as previously described (Guyenet and Wang, 2001; Wang et al., 2001). Fig. 1A, C highlight the location of the pre-BötC ventrally and the nucleus ambiguus dorsally in the ventrolateral medulla, consistent with our previous studies (Wei et al., 2010; Kang et al., 2017). NK1R immunoreactivity was distributed mainly on the surfaces of the somata and processes, clearly outlining the pre-BötC neurons. NK1R-immunoreactive (ir) neurons were oval, fusiform, or multipolar in shape, and small to medium in size with thin and long processes (Fig. 1B, D). NK1R-ir neurons expressed diverse intensities of CO reactivity. Densitometric measurements of CO reaction product of NK1R-ir neurons were plotted in Fig. 1E. A significant increase in CO reactivity was evident in the pre-BötC in dAIH group (0.53 ± 0.005), as compared to the normoxic control (0.46 ± 0.004, $P < 0.001$), indicating an increase in CO activity induced by dAIH.

3.2. Electron microscopic examination of CO activity in the pre-BötC in normoxic and dAIH groups

The electron microscopic images revealed that NK1R immunogold-silver particles were distributed mainly along the inner surface of the membrane in the somata (Fig. 2A, B) and dendrites (Figs. 2C, 5–8). The cytoplasm also had NK1R immunoreactivity (Fig. 2A, B). CO reaction product was expressed on the inner mitochondrial membrane, filling the intracristate space (Figs. 2, 5–8). Three categories of CO-reactive mitochondria (darkly, moderately, and lightly) were defined according to the previous description (Wong-Riley et al., 1989). Darkly reactive mitochondria had > 50% of the inner mitochondrial membrane and intracristate space bearing CO reaction product (solid arrows in Fig. 2B, C). Moderately reactive ones had < 50% of inner mitochondrial membrane and intracristate space covered with reaction product (half solid arrows in Fig. 2), and lightly reactive ones had little or no detectable reaction product (open arrow in Fig. 2). The intensity of CO reaction product reflected the relative level of CO activity. Of 681 dendritic mitochondria examined in NK1R-ir pre-BötC neurons in normoxic group, 50.8% (346/681) were moderately reactive, and the rest were

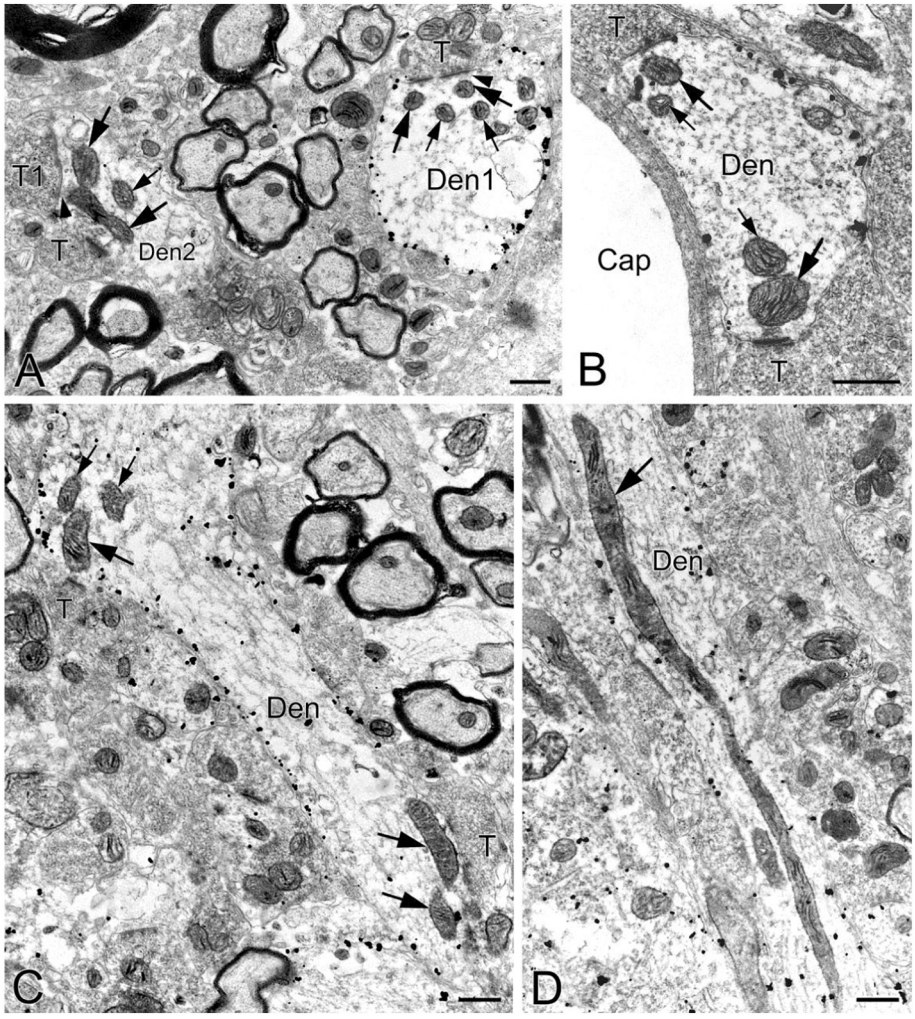

Fig. 6. Electron micrographs of CO-reactive mitochondria in pre-BötC dendrites in normoxic rats. Dendritic mitochondria were globular or ovoid in transverse sections (Den 1 in A, B). Thick arrows show mitochondria in close proximity to synapses. Thin arrows in A-C point to adjacent mitochondria. Arrowheads in A indicate flocculent or filament-like elements. An extremely long mitochondrion is present in a dendrite (D). Den: dendrite, T: terminal, Cap: capillary. Scale bars: 0.5 μm.

darkly (23.8%, 162/681) and lightly (25.4%, 173/681) reactive, whereas in the somata, lightly reactive ones (71.1%, 492/692) were predominate, and dark ones only accounted for a small proportion (3%, 21/692). dAIH challenge significantly increased the proportion of darkly reactive mitochondria to 48.3% (333/688) in dendrites and 13.4% (95/709) in the somata, and the light ones declined to 5.5% (38/688) in dendrites and 37.7% (267/709) in the somata (Fig. 3). The moderate ones (48.9%, 347/709) were also significantly increased in the somata in the dAIH group (Fig. 3). Consistently, densitometric measurements showed that dendritic mitochondria expressed higher levels of CO reactivity than those in the somata in both groups (Fig. 4). dAIH challenge significantly increased CO reactivity in dendrites (0.54 ± 0.008 in dAIH versus 0.46 ± 0.007 in normoxic group, $P < 0.001$) and the somata (0.36 ± 0.01 versus 0.27 ± 0.009, $P < 0.001$, Fig. 4), indicating an increase in CO activity induced by dAIH.

3.3. Dendritic mitochondrial ultrastructure in the pre-BötC in normoxic and dAIH groups

Mitochondria are interconnected and bioenergetically coupled to neuronal activity and neuroplasticity. Increased CO activity induced by dAIH in pre-BötC neurons may be accompanied by alterations in mitochondrial morphology or ultrastructure. We noted ultrastructural features of dendritic mitochondria and their correlations with synapses because postsynaptic activity requires the largest amount of ATP supply. Technically, NK1R immunogold-silver particles precisely outlined the somata and dendrites of the pre-BötC neurons, providing a morphological marker for us to define mitochondria within the specific nucleus.

Mitochondria in the somata were usually globular or ovoid in shape (0.49 ± 0.01 μm in length) with tubular or vesicular cristae in the pre-BötC (Fig. 2A, B). Dendritic mitochondria displayed some differences from those in the somata. They were generally slender and elongated in shape (0.92 ± 0.039 μm in length) with lamellar cristae, orienting longitudinally along dendritic shafts (Figs. 2C, 5A, C, 6C, 7A, B, D, 8A, B). Occasionally, extremely long mitochondria (> 8 μm) were visualized (Fig. 6D). In transverse sections, dendritic mitochondria were globular or ovoid in shape (0.25 ± 0.004 μm in length, Figs. 6A, B, 7C). A vast majority of dendritic mitochondria were confined to dendritic shafts (Figs. 2C, 5A–C, E, F, 6, 7, 8A, B). Dendritic spines rarely contained mitochondria (Fig. 5D, 8D). Dendritic mitochondria in association with synapses displayed some ultrastructural changes. First, mitochondria located in close proximity to synapses appeared to have undergone ultrastructural remodeling, such as local enlargement (thick arrow in Fig. 2C, arrows in Fig. 5C, E, F) or altered shapes (arrows in Fig. 5B, D). Fig. 5Bdisplays a mitochondrion seemingly extending into various directions. Similarly in Fig. 5D, a mitochondrion was tapered

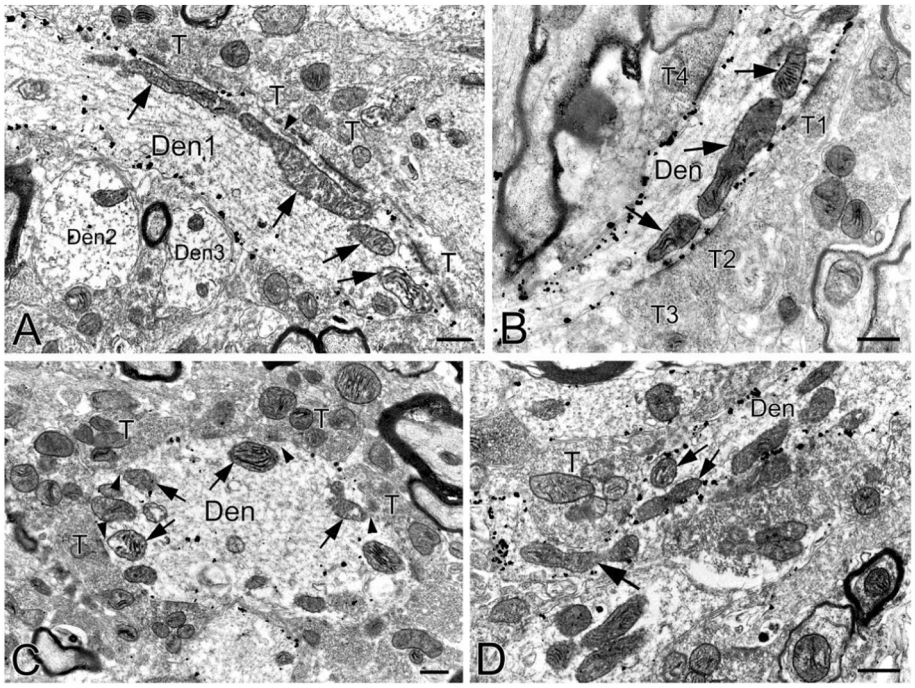

Fig. 7. Electron micrographs of CO-reactive mitochondria in pre-BötC dendrites of dAIH rats. Mitochondria were found mainly close to synapses (arrows in A), and they tended to aggregate next to multiple synapses rather than fewer ones (arrows in B). A tapered mitochondrion was observed in a narrow dendritic shaft, where it encountered a terminal (thick arrow in D). Flocculent or filament-like elements were identified (arrowheads in C). An endoplasmic reticulum was found between the mitochondrion and the postsynaptic membrane (arrowhead in A). Den: dendrite, T: terminal. Scale bars: 0.5 μm.

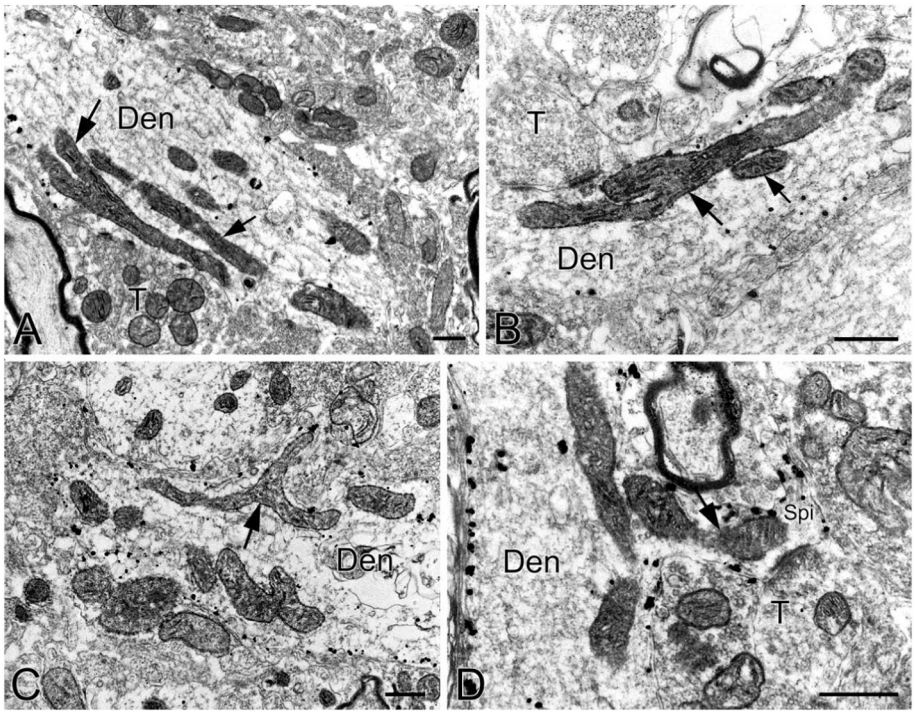

Fig. 8. Electron micrographs of CO-reactive mitochondria in pre-BötC dendrites of dAIH rats. Mitochondria with branching morphology were in close vicinity to synapses (thick arrows in A, B). Adjacent mitochondria were seen close to the branching ones (thin arrows in A, B). Notably, mitochondria were seen with an altered shape, next to a terminal (arrow in C) or extending into a dendritic spine (thick arrow in D). Den: dendrite, T: terminal, Spi: spine. Scale bars: 0.5 μm.

and appeared to extend toward a spine. Second, lamellar cristae with dark CO reactivity were observed at postsynaptic sites (Figs. 5A–E, 6A–C, 7). Third, flocculent or filament-like elements were found between mitochondria and the postsynaptic membrane (arrowheads in Figs. 5C, 6A, 7C), seemingly to anchor mitochondria to synapses. The endoplasmic reticulum was also found between the mitochondrion and the postsynaptic membrane (arrowhead in Fig. 7A). Fourth, dendritic mitochondria were positioned in close vicinity to synapses, and away from sites that lack synapses (arrows in Figs. 2C, 5A, E, 6, 7, 8A, B), and often they resided close to two or more synapses rather than only one (arrows in Figs. 5C, 6A, C, 7B). Fig. 6B presents four mitochondria distributed to two asymmetric synapses in a dendrite, two at each synapse. Furthermore, mitochondria were often arranged in tandem, with one facing and close to the synapse, and the other a short distance away (thin arrows in Figs. 5D, 6A–C, 8A, B). The followers may serve as a reservoir to ensure continuous energy supply.

3.4. Mitochondrial alterations in the pre-BötC induced by dAIH

Dendritic mitochondria manifested some changes in morphological connections with synapses in the pre-BötC following dAIH exposure. Indeed, the proportion of dendritic mitochondria in close proximity to synapses was significantly increased to 66.1% (455/688) in dAIH as compared to 53.9% (367/681) in normoxia, whereas the number of

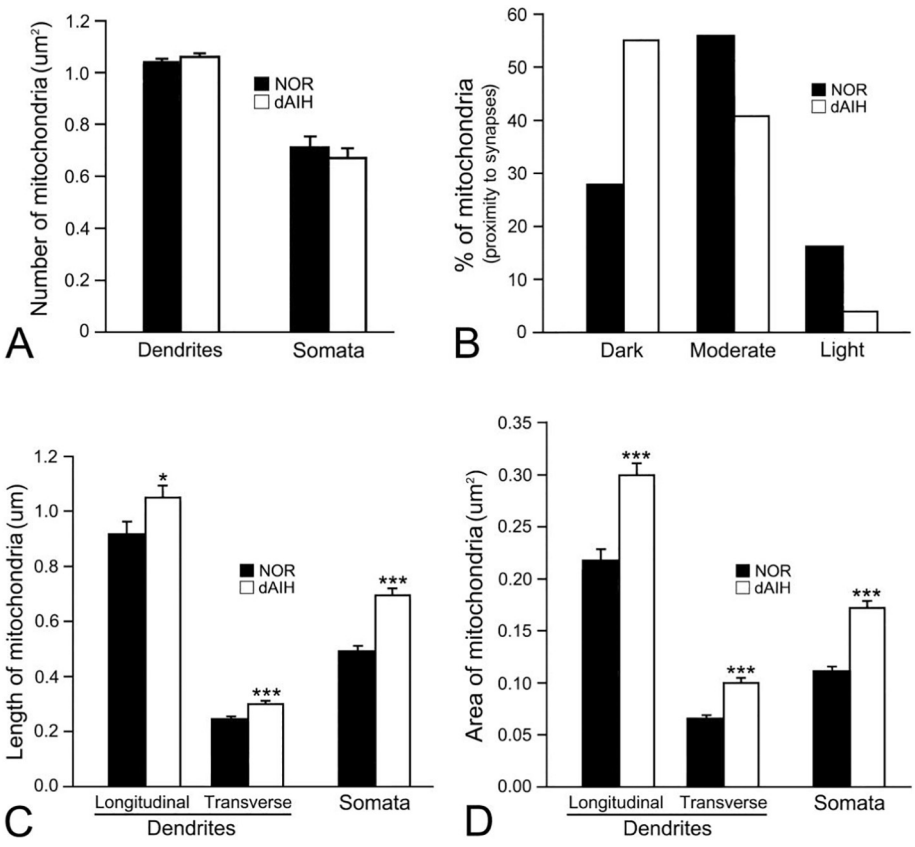

Fig. 9. Number, length and area of mitochondria in dendrites and the somata, and percent of CO-reactive mitochondria in close proximity to postsynaptic sites in the pre-BötC in normoxic and dAIH groups. The number of mitochondria showed no significant differences between two groups (A, Unpaired *t*-test, Dendrites: $t = 0.2779$, $p = 0.7813$; Somata: $t = 1.021$, $p = 0.3112$). The percent of darkly reactive mitochondria in close proximity to synapses were greater, and moderately and lightly reactive ones were less in the dAIH as compared to the normoxic group (B). dAIH challenge significantly increased the length (C) and area (D) of mitochondria in dendrites and somata (C, unpaired t-test, dendritic longitudinal mitochondria: $t = 2.305$, $p = 0.0215$; dendritic transverse mitochondria: $t = 5.492$, $p < 0.001$; somata: $t = 7.038$, $p < 0.001$; D, unpaired t-test, dendritic longitudinal mitochondria: $t = 4.263$, $p < 0.001$; dendritic transverse mitochondria: $t = 6.575$, $p < 0.001$; somata: $t = 9.068$, $p < 0.001$). *: $p < 0.05$, ***: $p < 0.001$.

mitochondria did not differ between the two groups (Fig. 9A). Of note, the majority of mitochondria (55.2%, 251/455) close to synapses were darkly reactive for CO activity, and a combination of darkly to moderately reactive mitochondria reached 96% (437/455) in the dAIH group, whereas in the normoxic control, most of the mitochondria (56.1%, 206/367) were moderately reactive for CO activity, and the darkly to moderately reactive ones accounted for 83.9% (308/367) (Fig. 9B). Additionally, the mean length of dendritic mitochondria was significantly increased in the dAIH group (1.05 ± 0.036 μm in longitudinal sections and 0.29 ± 0.005 μm in transverse sections), as compared to the normoxic control (0.92 ± 0.039 μm in longitudinal sections and 0.25 ± 0.004 μm in transverse sections, Fig. 9C). A similar increase was evident for somatic mitochondria in the dAIH group (0.69 ± 0.016 μm, Fig. 9C), which significantly increased the mean area of mitochondria (Fig. 9D). Branching mitochondria were identified with the larger area (Fig. 8A, B), a feature that was seldom observed in the normoxic group. Fig. 7D illustrates a mitochondrion that was tapered through a narrow dendritic shaft, which was contacted by a presynaptic terminal. Fig. 8C, D illustrate portions of mitochondria that faced a presynaptic terminal or entered into a dendritic spine, representing a morphological characteristic of mitochondria-spine communication.

4. Discussion

The present study demonstrates possible adaptive changes in mitochondrial ultrastructure and CO activity in pre-BötC neurons in response to respiratory neuroplasticity induced by dAIH. First, dAIH challenge significantly increased CO activities in the pre-BötC. The increased CO activity was correlated with an increase in the number of darkly reactive mitochondria and a decline in lightly reactive ones, especially in postsynaptic dendrites. Darkly CO reactive mitochondria were much more distributed to synapses after dAIH exposure. Second, the mean length and area of mitochondria were significantly increased in the dAIH group, implying an increased cristae surface area for the generation of ATP. Finally, mitochondria manifested an apparent fine structural remodeling, including locally enlarged or branching mitochondria and extending into the dendritic spines. The cristae of mitochondria were mainly in lamellar arrangement, and flocculent or filament-like elements were evident between the mitochondria and the postsynaptic membrane. These morphological adjustments, together with changes in their CO activity, implicate mitochondria in the pre-BötC to act dynamically in response to respiratory neuroplasticity.

4.1. Cytochrome c oxidase (CO) activity in the pre-BötC

CO, a terminal enzyme of the mitochondrial electron transport chain, serves as a sensitive and reliable marker of neuronal oxidative capacity and energy metabolism, and is tightly coupled to neuronal activity (Wong-Riley, 1989, 2012). Indeed, gray matter consistently manifests greater CO activity than white matter, and nuclear groups with high levels of spontaneous and synaptic activities show strong CO activities (Wong-Riley, 1989). The complex subcellular compartments of dendrites, axons, and axonal terminals in neurons function differently and expend energy differently, thereby their CO activities are not homogeneous among the compartments. Dendrites manifest high CO activity because a large fraction of energy expenditure is postsynaptically driven in dendrites, whereas axonal trucks, especially myelinated axons consume very little energy and possess low levels of CO activities (Wong-Riley, 1989, 2012).

CO histochemistry with quantitative optical densitometry has been widely used to demonstrate neuronal activities at regional, cellular and subcellular levels (Hevner and Wong-Riley, 1989; Wong-Riley et al., 1989; Liu and Wong-Riley, 2001; Liu et al., 2001). In the present study, we first combined CO histochemistry with NK1R immunogold-silver cytochemistry to determine CO activities in the pre-BötC at ultrastructural levels. We found that dendrites presented higher CO activity than the somata in NK1R-ir neurons of the pre-BötC. Darkly and

moderately CO reactive mitochondria were predominant in dendrites, whereas lightly reactive ones were prevalent in the somata. dAIH exposure markedly increased darkly reactive mitochondria in dendrites and moderately ones in the somata, indicating increased CO activity, particularly in dendrites. The pre-BötC is composed mainly of glutamatergic neurons, some of which have intrinsic membrane properties that can be fully evoked by glutamatergic synaptic inputs to shape inspiratory drive potentials (Gray et al., 2010; Koizumi et al., 2016). It is likely that dAIH challenge stimulates glutamatergic microcircuits in the pre-BötC, especially in postsynaptic dendrites that require additional energy consumption for respiratory LTF expression.

4.2. Ultrastructural changes in dendritic mitochondria within the pre-BötC

Mitochondria are essential for energy supply and Ca^{2+} buffering homeostasis in cells, especially in neurons that mitochondria provide most of the ATP for neuronal functions (Harris et al., 2012). Synapses are the primary sites of ATP consumption, where mitochondria supply around 93% of the ATP, while glycolysis generates only 7% of the ATP (Harris et al., 2012). A majority of energy is used for reversing ion influxes underlying synaptic and action potential signaling, thus mitochondria are located close to active synapses to support neuronal activities (Harris et al., 2012; Barnhart, 2016). In addition, mitochondria maintain calcium homeostasis at synapses by sequestering intracellular Ca^{2+} for synaptic activities (Kang et al., 2008; Cai et al., 2011). Elevated intracellular Ca^{2+} during sustained synaptic activities recruits mitochondria to synapses (Yi et al., 2004; Sheng, 2014). Therefore, mitochondria are highly dynamic organelles that continuously change in structure and function in response to altered synaptic strength and activities (Cserep et al., 2018). Functional demands of mitochondria differ in dendrites and axons. Dendrites have a greater proportion of highly charged and more metabolically active mitochondria than axons (Overly et al., 1996). However, dendritic mitochondria are less explored especially at the ultrastructural level.

The present study illustrates fine structural characteristics of mitochondria in the pre-BötC. We found that dendritic mitochondria were in close proximity to synapses, and they could extend into dendritic spines. Mitochondrial extending into various directions in dendritic shafts, as illustrated in Fig. 5B, may reflect their morphological plasticity to cope with high energy demand at synapses. In addition, mitochondria near the postsynaptic sites manifested fine structural remodeling, including locally enlarged mitochondria, lamellar cristae with dark CO reactivity, and flocculent or filament-like elements that appeared to connect mitochondria to the postsynaptic membrane. Indeed, we found that the intracristate space was filled with CO reaction product and lamellar cristae with high CO activity, implying a high respiratory and ATP-generating efficiency (Song et al., 2013; Cogliati et al., 2016). Moreover, locally enlarged mitochondria at synapses can provide greater surface area for cristae extension and arrangement, further increasing the respiratory efficiency. Furthermore, flocculent or filament-like elements seemed to tether mitochondria to the postsynaptic membrane. The morphological characteristics and positioning may suggest mitochondrial docking, as dendritic mitochondria are much more stable than axonal ones (Overly et al., 1996), and stationary or docked mitochondria provide stable and continuous ATP supply to maintain energy homeostasis at synapses (Sheng, 2014). Actin, neurofilament and microtubule cytoskeletal elements are involved in anchoring mitochondria in both axons and dendrites (MacAskill and Kittler, 2010). Interactions between mitochondria and neurofilaments rely on the mitochondrial membrane potential to specifically stabilize active mitochondria at a given location (Wagner et al., 2003). Miro, a mitochondrial outer membrane protein is also required to position mitochondria at postsynaptic sites via a calcium-dependent mechanism with activation of glutamate receptors (Macaskill et al., 2009). Whether flocculent or filament-like elements found in the present study are relevant to cytoskeletal proteins or docking proteins remain to be explored.

4.3. Plasticity of dendritic mitochondria and LTF in the pre-BötC

The pre-BötC is known to contribute to respiratory plasticity, which is evoked by repetitive hypoxia, leading to adaptive or detrimental consequences depending on the severity and duration of hypoxia (Dale-Nagle et al., 2010; Dale et al., 2014). A severe intermittent hypoxic challenge has been demonstrated to increase irregular outputs and destabilize rhythmogenesis in the isolated pre-BötC, resulting in an intermittent transmission failure to the hypoglossal motor nucleus (Garcia 3rd et al., 2016, 2017). On the contrary, a mild dAIH protocol as used in the present study actually augments respiratory motor output, referring to as LTF expression that is beneficial and adaptive without causing pathological morbidities (Dale et al., 2014; Navarrete-Opazo et al., 2015; Dougherty et al., 2017).

Mitochondria are highly plastic organelles involved in the modulation of neuroplasticity (Cheng et al., 2010). In axonal terminals, mitochondria have been implicated in certain forms of short-term synaptic plasticity by sequestering presynaptic Ca^{2+} transients and modulating Ca^{2+} signaling (Kang et al., 2008). Mitochondria are also required for vesicular release following long-term potentiation stimulation and are correlated with synaptic strength (Sun et al., 2013). Increased synaptic performance is closely coupled to mitochondrial ultrastructural plasticity, including increased volume, cristae density, and cristae lamellarity in axonal mitochondria (Smith et al., 2016; Cserep et al., 2018). We found that dAIH challenge significantly increased the mean length and area of mitochondria in dendrites and the somata in the pre-BötC. Elongation of mitochondria is considered to be an active mechanism in association with increases in mitochondrial bioenergetic efficiency (Cogliati et al., 2016). These mitochondria possess increases in cristae number, dimerization, and activity of ATP synthase, resulting in increased efficiency of ATP synthesis (Gomes et al., 2011; Liesa and Shirihai, 2013). Elongated branching mitochondria with increases in mean area and CO activity induced by dAIH are consistent with a robust ATP generating capacity in the pre-BötC.

Additionally, mitochondria are accumulated at pre-BötC synapses following dAIH challenge. Approximately two thirds of mitochondria, mostly darkly reactive for CO, were distributed in close proximity to synapses in the dAIH group, whereas in normoxia, proportion of mitochondria in close proximity to synapses was 53.9%, of which < 30% were darkly reactive. It is well known that mitochondria are transported to regions where the ATP consumption is high and where the ATP/ADP ratio is low (Wong-Riley, 1989; Overly et al., 1996). Tetanic stimulation of an intact *Drosophila* nervous system triggers a fast delivery of mitochondria to synapses, facilitating postsynaptic potentiation. Inhibition of electron transport chain complex I suppresses mitochondrial transport and abolishes the synaptic potentiation, whereas an increase in mitochondrial ATP synthesis in neurons enhances movements of mitochondria to synapses (Tong, 2007), indicating a critical role of ATP generation in synaptic plasticity. Indeed, we found a majority of mitochondria with dark CO reactivity positioned at postsynaptic sites in the pre-BötC, suggesting a locally high ATP consumption. Thus, dAIH challenge may stimulate glutamatergic microcircuits in the pre-BötC that demand augmented energy to fuel increased postsynaptic activities, such as the reversal of ion movements following the opening of ion channels, and activation of the phosphorylation cascades for Ca^{2+} influx through glutamatergic receptors. Activation of NMDA receptors and increases in Ca^{2+} influx may further inhibit mitochondrial motility and arrest mitochondria to postsynaptic sites (Yi et al., 2004; Nasrallah and Horvath, 2014), to sustain continuous energy supply for respiratory LTF expression.

Dendritic spines very rarely contain mitochondria in mature neurons, except large spines such as CA3 pyramidal neurons (Popov et al., 2005). Studies on cultured embryonic neurons via time-lapse imaging have shown the movement of mitochondria into dendritic protrusions

that correlates with morphological plasticity of developing spines (Li et al., 2004). The mitochondrion-to-spine signaling displays high spatiotemporal specificity to decode complex signaling from spines for full structural LTP expression (Fu et al., 2017). The present study is the first one that demonstrated ultrastructural evidence of spine-mitochondrion communications in the pre-BötC in adult animals. The morphological features manifest a high degree of structural plasticity in mitochondria, as exampled in Fig. 8D. ATP is thought to diffuse into the spines to provide energy for synaptic activity. Our ultrastructural evidence suggests that mitochondria are able to extend into spines to meet local synaptic energy needs and to sense Ca^{2+} homeostasis/signaling under dAIH challenge, thereby contributing to respiratory LTF.

In conclusion, dendritic mitochondria are robustly dynamic in response to respiratory LTF in the pre-BötC. dAIH challenge evokes diverse ultrastructural plasticity in the shape, area, and distribution of mitochondria with a significant increase in CO activity. All plastic changes are in synchrony with active mitochondrial bioenergetics, leading to reinforced energy production and biosensor for Ca^{2+} buffering and signaling that contribute to the LTF expression.

Acknowledgements

This study was supported by Natural Science Foundation of China (grants: 31171102, 31471097) to YYL. We thank Mr. Lo YM for his technical assistance.

Conflict of interest disclosure

The authors declare no conflict of interest.

References

Barnett, W.H., Abdala, A.P., Paton, J.F., Rybak, I.A., Zoccal, D.B., Molkov, Y.I., 2017. Chemoreception and neuroplasticity in respiratory circuits. Exp. Neurol. 287, 153–164.
Barnhart, E.L., 2016. Mechanics of mitochondrial motility in neurons. Curr. Opin. Cell Biol. 38, 90–99.
Billups, B., Forsythe, I.D., 2002. Presynaptic mitochondrial calcium sequestration influences transmission at mammalian central synapses. J. Neurosci. 22, 5840–5847.
Cai, Q., Davis, M.L., Sheng, Z.H., 2011. Regulation of axonal mitochondrial transport and its impact on synaptic transmission. Neurosci. Res. 70, 9–15.
Cheng, A., Hou, Y., Mattson, M.P., 2010. Mitochondria and neuroplasticity. ASN Neuro. 2, e00045.
Cogliati, S., Enriquez, J.A., Scorrano, L., 2016. Mitochondrial cristae: where beauty meets functionality. Trends Biochem. Sci. 41, 261–273.
Cserep, C., Posfai, B., Schwarcz, A.D., Denes, A., 2018. Mitochondrial ultrastructure is coupled to synaptic performance at axonal release sites. eNeuro 5.
Dale, E.A., Ben Mabrouk, F., Mitchell, G.S., 2014. Unexpected benefits of intermittent hypoxia: enhanced respiratory and nonrespiratory motor function. Physiology (Bethesda) 29, 39–48.
Dale-Nagle, E.A., Hoffman, M.S., MacFarlane, P.M., Satriotomo, I., Lovett-Barr, M.R., Vinit, S., Mitchell, G.S., 2010. Spinal plasticity following intermittent hypoxia: implications for spinal injury. Ann. N. Y. Acad. Sci. 1198, 252–259.
Dougherty, B.J., Terada, J., Springborn, S.R., Vinit, S., MacFarlane, P.M., Mitchell, G.S., 2018. Daily acute intermittent hypoxia improves breathing function with acute and chronic spinal injury via distinct mechanisms. Respir. Physiol. Neurobiol. 256, 50–57.
Feldman, J.L., Del Negro, C.A., Gray, P.A., 2013. Understanding the rhythm of breathing: so near, yet so far. Annu. Rev. Physiol. 75, 423–452.
Fu, Z.X., Tan, X., Fang, H., Lau, P.M., Wang, X., Cheng, H., Bi, G.Q., 2017. Dendritic mitoflash as a putative signal for stabilizing long-term synaptic plasticity. Nat. Commun. 8, 31.
Garcia 3rd, A.J., Zanella, S., Dashevskiy, T., Khan, S.A., Khuu, M.A., Prabhakar, N.R., Ramirez, J.M., 2016. Chronic intermittent hypoxia alters local respiratory circuit function at the level of the preBotzinger complex. Front. Neurosci. 10, 4.
Garcia 3rd, A.J., Dashevskiy, T., Khuu, M.A., Ramirez, J.M., 2017. Chronic intermittent hypoxia differentially impacts different states of inspiratory activity at the level of the prebotzinger complex. Front. Physiol. 8, 571.
Gomes, L.C., Di Benedetto, G., Scorrano, L., 2011. During autophagy mitochondria elongate, are spared from degradation and sustain cell viability. Nat. Cell Biol. 13, 589–598.
Gray, P.A., Rekling, J.C., Bocchiaro, C.M., Feldman, J.L., 1999. Modulation of respiratory frequency by peptidergic input to rhythmogenic neurons in the preBotzinger complex. Science 286, 1566–1568.
Gray, P.A., Janczewski, W.A., Mellen, N., McCrimmon, D.R., Feldman, J.L., 2001. Normal breathing requires preBotzinger complex neurokinin-1 receptor-expressing neurons. Nat. Neurosci. 4, 927–930.
Gray, P.A., Hayes, J.A., Ling, G.Y., Llona, I., Tupal, S., Picardo, M.C., Ross, S.E., Hirata, T., Corbin, J.G., Eugenin, J., Del Negro, C.A., 2010. Developmental origin of preBotzinger complex respiratory neurons. J. Neurosci. 30, 14883–14895.
Gunter, T.E., Buntinas, L., Sparagna, G., Eliseev, R., Gunter, K., 2000. Mitochondrial calcium transport: mechanisms and functions. Cell Calcium 28, 285–296.
Guyenet, P.G., Wang, H., 2001. Pre-Botzinger neurons with preinspiratory discharges "in vivo" express NK1 receptors in the rat. J. Neurophysiol. 86, 438–446.
Harris, J.J., Jolivet, R., Attwell, D., 2012. Synaptic energy use and supply. Neuron 75, 762–777.
Hevner, R.F., Wong-Riley, M.T., 1989. Brain cytochrome oxidase: purification, antibody production, and immunohistochemical/histochemical correlations in the CNS. J. Neurosci. 9, 3884–3898.
Kang, J.S., Tian, J.H., Pan, P.Y., Zald, P., Li, C., Deng, C., Sheng, Z.H., 2008. Docking of axonal mitochondria by syntaphilin controls their mobility and affects short-term facilitation. Cell 132, 137–148.
Kang, J.J., Liang, W.H., Lam, C.S., Huang, X.F., Yang, S.J., Wong-Riley, M.T., Fung, M.L., Liu, Y.Y., 2017. Catecholaminergic neurons in synaptic connections with pre-Botzinger complex neurons in the rostral ventrolateral medulla in normoxic and daily acute intermittent hypoxic rats. Exp. Neurol. 287, 165–175.
Koizumi, H., Mosher, B., Tariq, M.F., Zhang, R., Koshiya, N., Smith, J.C., 2016. Voltage-dependent rhythmogenic property of respiratory pre-botzinger complex glutamatergic, dbx1-derived, and somatostatin-expressing neuron populations revealed by graded optogenetic inhibition. eNeuro 3.
Li, Z., Sheng, M., 2012. Caspases in synaptic plasticity. Mol. Brain 5, 15.
Li, Z., Okamoto, K., Hayashi, Y., Sheng, M., 2004. The importance of dendritic mitochondria in the morphogenesis and plasticity of spines and synapses. Cell 119, 873–887.
Liesa, M., Shirihai, O.S., 2013. Mitochondrial dynamics in the regulation of nutrient utilization and energy expenditure. Cell Metab. 17, 491–506.
Lieske, S.P., Thoby-Brisson, M., Telgkamp, P., Ramirez, J.M., 2000. Reconfiguration of the neural network controlling multiple breathing patterns: eupnea, sighs and gasps [see comment]. Nat. Neurosci. 3, 600–607.
Liu, Y.Y., Wong-Riley, M.T., 2001. Developmental study of cytochrome oxidase activity in the brain stem respiratory nuclei of postnatal rats. J. Appl. Physiol. 1985 (90), 685–694.
Liu, Y.Y., Wong-Riley, M.T., Liu, H.L., Jia, Y., Jiao, X.Y., Wang, C.T., You, S.W., Ju, G., 2001. Increase in cytochrome oxidase activity in regenerating nerve fibers of hemitransected spinal cord in the rat. Neuroreport 12, 3239–3242.
MacAskill, A.F., Kittler, J.T., 2010. Control of mitochondrial transport and localization in neurons. Trends Cell Biol. 20, 102–112.
Macaskill, A.F., Rinholm, J.E., Twelvetrees, A.E., Arancibia-Carcamo, I.L., Muir, J., Fransson, A., Aspenstrom, P., Attwell, D., Kittler, J.T., 2009. Miro1 is a calcium sensor for glutamate receptor-dependent localization of mitochondria at synapses. Neuron 61, 541–555.
Mitchell, G.S., Johnson, S.M., 2003. Neuroplasticity in respiratory motor control. J. Appl. Physiol. 1985 (94), 358–374.
Mitchell, G.S., Baker, T.L., Nanda, S.A., Fuller, D.D., Zabka, A.G., Hodgeman, B.A., Bavis, R.W., Mack, K.J., Olson Jr., E.B., 2001. Invited review: Intermittent hypoxia and respiratory plasticity. J. Appl. Physiol. 1985 (90), 2466–2475.
Nasrallah, C.M., Horvath, T.L., 2014. Mitochondrial dynamics in the central regulation of metabolism. Nat. Rev. Endocrinol. 10, 650–658.
Navarrete-Opazo, A., Vinit, S., Dougherty, B.J., Mitchell, G.S., 2015. Daily acute intermittent hypoxia elicits functional recovery of diaphragm and inspiratory intercostal muscle activity after acute cervical spinal injury. Exp. Neurol. 266, 1–10.
Overly, C.C., Rieff, H.I., Hollenbeck, P.J., 1996. Organelle motility and metabolism in axons vs dendrites of cultured hippocampal neurons. J. Cell Sci. 109, 971–980.
Popov, V., Medvedev, N.I., Davies, H.A., Stewart, M.G., 2005. Mitochondria form a filamentous reticular network in hippocampal dendrites but are present as discrete bodies in axons: a three-dimensional ultrastructural study. J. Comp. Neurol. 492, 50–65.
Ruggiero, A., Aloni, E., Korkotian, E., Zaltsman, Y., Oni-Biton, E., Kuperman, Y., Tsoory, M., Shachnai, L., Levin-Zaidman, S., Brenner, O., Segal, M., Gross, A., 2017. Loss of forebrain MTCH2 decreases mitochondria motility and calcium handling and impairs hippocampal-dependent cognitive functions. Sci. Rep. 7, 44401.
Sheng, Z.H., 2014. Mitochondrial trafficking and anchoring in neurons: New insight and implications. J. Cell Biol. 204, 1087–1098.
Smith, J.C., Ellenberger, H.H., Ballanyi, K., Richter, D.W., Feldman, J.L., 1991. Pre-Botzinger complex: a brainstem region that may generate respiratory rhythm in mammals. Science 254, 726–729.
Smith, H.L., Bourne, J.N., Cao, G., Chirillo, M.A., Ostroff, L.E., Watson, D.J., Harris, K.M., 2016. Mitochondrial support of persistent presynaptic vesicle mobilization with age-dependent synaptic growth after LTP. elife 5.
Song, D.H., Park, J., Maurer, L.L., Lu, W., Philbert, M.A., Sastry, A.M., 2013. Biophysical significance of the inner mitochondrial membrane structure on the electrochemical potential of mitochondria. Phys. Rev. E Stat. Nonlinear Soft Matter Phys. 88, 062723.
Stowers, R.S., Megeath, L.J., Gorska-Andrzejak, J., Meinertzhagen, I.A., Schwarz, T.L., 2002. Axonal transport of mitochondria to synapses depends on Milton, a novel Drosophila protein. Neuron 36, 1063–1077.
Sun, T., Qiao, H., Pan, P.Y., Chen, Y., Sheng, Z.H., 2013. Motile axonal mitochondria contribute to the variability of presynaptic strength. Cell Rep. 4, 413–419.
Tong, J.J., 2007. Mitochondrial delivery is essential for synaptic potentiation. Biol. Bull. 212, 169–175.
Wagner, O.I., Lifshitz, J., Janmey, P.A., Linden, M., McIntosh, T.K., Leterrier, J.F., 2003. Mechanisms of mitochondria-neurofilament interactions. J. Neurosci. 23, 9046–9058.

Wang, H., Stornetta, R.L., Rosin, D.L., Guyenet, P.G., 2001. Neurokinin-1 receptor-immunoreactive neurons of the ventral respiratory group in the rat. J. Comp. Neurol. 434, 128–146.
Wei, X.Y., Liu, J.P., Zhao, C.H., Ju, G., Wong-Riley, M.T., Liu, Y.Y., 2010. Expressions of 5-HT/5-HT(2A) receptors and phospho-protein kinase C theta in the pre-Botzinger complex in normal and chronic intermittent hypoxic rats. Neuroscience 168, 61–73.
Wong-Riley, M.T., 1989. Cytochrome oxidase: an endogenous metabolic marker for neuronal activity. Trends Neurosci. 12, 94–101.
Wong-Riley, M.T., 2012. Bigenomic regulation of cytochrome c oxidase in neurons and the tight coupling between neuronal activity and energy metabolism. Adv. Exp. Med. Biol. 748, 283–304.
Wong-Riley, M.T., Tripathi, S.C., Trusk, T.C., Hoppe, D.A., 1989. Effect of retinal impulse blockage on cytochrome oxidase-rich zones in the macaque striate cortex: I. Quantitative electron-microscopic (EM) analysis of neurons. Vis. Neurosci. 2, 483–497.
Xing, T., Fong, A.Y., Bautista, T.G., Pilowsky, P.M., 2013. Acute intermittent hypoxia induced neural plasticity in respiratory motor control. Clin. Exp. Pharmacol. Physiol. 40, 602–609.
Yi, M., Weaver, D., Hajnoczky, G., 2004. Control of mitochondrial motility and distribution by the calcium signal: a homeostatic circuit. J. Cell Biol. 167, 661–672.